Coherent and Differential Space-Time Shift Keying: A Dispersion Matrix Approach

Shinya Sugiura, *Member, IEEE,* Sheng Chen, *Fellow, IEEE,* and Lajos Hanzo, *Fellow, IEEE*

***Abstract*—Motivated by the recent concept of Spatial Modulation (SM), we propose a novel Space-Time Shift Keying (STSK) modulation scheme for Multiple-Input Multiple-Output (MIMO) communication systems, where the concept of SM is extended to include both the space and time dimensions, in order to provide a general shift-keying framework. More specifically, in the proposed STSK scheme one out of Q dispersion matrices is activated during each transmitted block, which enables us to strike a flexible diversity and multiplexing tradeoff. This is achieved by optimizing both the space-time block duration as well as the number of the dispersion matrices in addition to the number of transmit and receive antennas. We will demonstrate that the resultant equivalent system model does not impose any Inter-Channel Interference (ICI), and hence the employment of single-stream Maximum Likelihood (ML) detection becomes realistic at a low-complexity. Furthermore, we propose a Differential STSK (DSTSK) scheme, assisted by the Cayley unitary transform, which does not require any Channel State Information (CSI) at the receiver. Here, the usual error-doubling, caused by the differential decoding, gives rise to 3-dB performance penalty in comparison to Coherent STSK (CSTSK). Additionally, we introduce an enhanced CSTSK scheme, which avoids the requirement of Inter-Antenna Synchronization (IAS) between the RF chains associated with the transmit Antenna Elements (AEs) by imposing a certain constraint on the dispersion matrix design, where each column of the dispersion matrices includes only a single non-zero component. Moreover, according to the turbo-coding principle, the proposed CSTSK and DSTSK schemes are combined with multiple serially concatenated codes and an iterative bit-to-symbol soft-demapper. More specifically, the associated STSK parameters are optimized with the aid of EXtrinsic Information Transfer (EXIT) charts, for the sake of achieving a near-capacity performance.**

***Index Terms*—Diversity and multiplexing tradeoff, space-time coding, spatial modulation, linear dispersion code, maximum likelihood detection, multiple antenna array, non-coherent detection.**

I. Introduction

MULTIPLE-antenna-assisted wireless communication systems have attracted substantial attention due to their potentials to achieve reliable high-rate transmission [1]. For example, the Vertical Bell Laboratories Layered Space-Time (V-BLAST) [2] scheme is capable of attaining a high multiplexing gain at the cost of a substantial decoding complexity imposed by mitigating the effects of Inter-Channel Interference (ICI). By contrast, Space-Time Block Codes (STBCs) [3], [4] were developed to achieve the maximum attainable diversity order, although the maximum bandwidth efficiency of the full-rate orthogonal STBCs is limited to one bit per symbol duration. Furthermore, Hassibi and Hochwald [5] proposed the unified space-time transmission architecture of Linear Dispersion Codes (LDCs), which subsumes both the V-BLAST and Alamouti's STBC scheme in its ultimate form and it is capable of striking a flexible tradeoff between the achievable diversity and multiplexing gains. Additionally, in [6] the differential-encoding assisted counterpart of LDCs was introduced in order to enable non-coherent detection at the receiver in the absence of CSI, which was referred to as Differential LDC (DLDC).

Recently, the sophisticated concept of Spatial Modulation (SM) [7]–[9] and Space-Shift Keying (SSK) [10][1] was invented for Multiple-Input Multiple-Output (MIMO) communication systems. The key idea is the activation of one of a total of M Antenna Elements (AEs) at each symbol duration, leading to an additional means of conveying source information, while removing the effects of ICI. Hence, this arrangement allows the employment of low-complexity single-antenna-based Maximum Likelihood (ML) detection, while V-BLAST requires the potentially excessive-complexity joint detection of multiple antennas' signals. This advantage becomes even more dominant in a rank-deficient scenario, where the number of transmit antennas is higher than that of the receive antennas and the channel-matrix becomes non-invertible. Therefore, either an increased-complexity non-linear detector has to be invoked or a substantial performance degradation is imposed on Spatial Division Multiplexing (SDM). As a result, it was demonstrated in [7]–[10] that SM/SSK has the potential of outperforming other MIMO arrangements, such as V-BLAST and Alamouti's STBC schemes.

On the other hand, since SM/SSK adopted V-BLAST's high-rate architecture, which was designed for achieving a multiplexing gain, rather than diversity gain, it has to rely on the employment of multiple DownLink (DL) receive AEs for the sake of combating the effects of fading channels. However, accommodating multiple DL elements imposes challenges, when transmitting to mobiles in DL scenarios. Additionally, when aiming for a linear increase in the transmission rate, the number of transmit antennas employed in the context of [7]–[10] has to be increased exponentially. We will circumvent this problem by introducing a new solution. Furthermore, a

Paper approved by C. Tellambura, the Editor for Multicarrier Systems of the IEEE Communications Society. Manuscript received November 26, 2009; revised April 8, 2010 and June 23, 2010.

The authors are with the School of Electronics and Computer Science, University of Southampton, Southampton, SO17 1BJ, UK (e-mail: {ss07r, sqc, lh}@ecs.soton.ac.uk). S. Sugiura is also with the Toyota Central Research and Development Laboratories, Inc., Aichi 480-1192, Japan (e-mail: sugiura@mosk.tytlabs.co.jp).

The financial support of the EU under the auspices of the Optimix project and of the EPSRC UK is gratefully acknowledged.

Digital Object Identifier 10.1109/TCOMM.2010.093010.090730

[1]As noted in [10], the SSK scheme can be viewed as the special case of the SM, where the presence or absence of energy allocated to a specific antenna conveys source information.

coherently detected SM/SSK scheme requires Channel State Information (CSI) at the receiver, although it is a challenging task to acquire accurate CSI for high-speed vehicles, which may require a high pilot overhead and imposes a substantial processing complexity. The resultant CSI estimation error is expected to erode the achievable performance.

Against this background the novel contributions of this paper are as follows:

1) Inspired by the SM/SSK scheme, we propose the novel concept of Space-Time Shift Keying (STSK) modulation, which constitutes a generalized shift-keying architecture utilizing both the space as well as time dimensions and hence includes the SM and SSK schemes as special cases. More specifically, the STSK scheme is based on the activation of Q number of appropriately indexed space-time dispersion matrices within each STSK block duration, rather than that of the indexed antennas at each symbol duration, as in the SM/SSK scheme of [7]–[10]. As a benefit of its high degree of design-freedom, our STSK scheme is capable of striking a flexible diversity versus multiplexing gain tradeoff, which is achieved by optimizing both the number and size of the dispersion matrices as well as the number of transmit and receive antennas. More specifically, our STSK scheme is capable of exploiting both transmit as well as receive diversity gains, unlike the conventional SM and SSK schemes, which can only attain receive diversity gain.[2] Furthermore, since no ICI is imposed by the resultant equivalent system model of the STSK scheme, the employment of single-antenna-based ML detection becomes realistic. Additionally, we introduce an improved STSK structure, which enables us to dispense with any symbol-level time-synchronization between the RF chains associated with the transmit AEs, similarly to the SM/SSK scheme.
2) As the extension of the above-mentioned Coherent STSK (CSTSK) scheme, we introduce a Differentially-encoded STSK (DSTSK) arrangement, assisted by the Cayley unitary transform based technique of [6], which does not require any CSI estimation at the receiver. More specifically, by employing the Cayley transform in the proposed DSTSK scheme we arrive at a linearized equivalent system model, which is common with that of the CSTSK scheme. Hence the DSTSK scheme retains the fundamental benefits of the CSTSK scheme, although naturally, the corresponding non-coherent receiver suffers from the well-known performance loss compared to its coherent counterpart. We note that while complex-valued constellations may be used in the CSTSK scheme in conjunction with appropriate dispersion-matrix activation, those of the DSTSK scheme are limited to real-valued constellations.
3) Moreover, according to the turbo-coding principle [12], our CSTSK and DSTSK schemes are extended to include three serially concatenated codes, while employing three-stage iterative detection at the receiver for the sake of achieving a near-capacity performance. Their iterative behaviour as well as maximum achievable capacity are investigated with the aid of EXtrinsic Information Transfer (EXIT) charts [13].

[2] After the submission of this paper, the (2×1)-element SM scheme capable of achieving a transmit diversity gain was also proposed in [11].

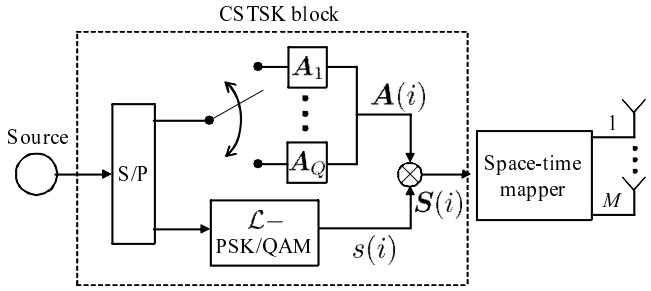

Fig. 1. Transmitter structure of our coherent STSK scheme.

The remainder of this paper is organized as follows. Section II outlines the concept of STSK modulation, which is then extended to include the turbo-coding principle in Section III. The optimization criterion used for the design of the dispersion matrices is provided in Section IV. In Section V we provide our performance results. Finally, we conclude this paper in Section VI.

II. Space-Time Shift Keying Modulation

In this contribution we consider an $(M\times N)$-element MIMO system, where M AEs are employed at the transmitter, while the receiver is equipped with N AEs, while assuming a frequency-flat Rayleigh fading environment. In general the block-based system model can be described as

$$\boldsymbol{Y}(i)=\boldsymbol{H}(i)\boldsymbol{S}(i)+\boldsymbol{V}(i), \tag{1}$$

where $\boldsymbol{Y}(i)\in\mathcal{C}^{N\times T}$ represents the received signals and $\boldsymbol{S}(i)\in\mathcal{C}^{M\times T}$ denotes the space-time signals and the mth row's elements are transmitted from the mth antenna, while i indicates the STSK block index. Furthermore, $\boldsymbol{H}(i)\in\mathcal{C}^{N\times M}$ and $\boldsymbol{V}(i)\in\mathcal{C}^{N\times T}$ denote the channel and noise components, each obeying the complex-valued zero-mean Gaussian distribution of $\mathcal{CN}(0,1)$ and of $\mathcal{CN}(0,N_0)$, respectively, where N_0 represents the noise variance.

In the rest of this section, we introduce two novel schemes, namely the CSTSK and DSTSK modulation arrangements. Here, we also present a modified CSTSK arrangement, which does not require any IAS between the RF antenna circuits at the transmitter. Furthermore, the decoding complexity of our CSTSK and DSTSK schemes as well as the maximum achievable diversity order of our CSTSK scheme are also derived.

A. Coherent STSK Scheme

Fig. 1 depicts the transmitter structure of our CSTSK scheme, where Q dispersion matrices $\boldsymbol{A}_q\in\mathcal{C}^{M\times T}$ $(q=1,\cdots,Q)$ are pre-assigned in advance of any transmission. A total of $\log_2(Q\cdot\mathcal{L})$ source bits are mapped to each space-time block $\boldsymbol{S}(i)\in\mathcal{C}^{M\times T}$ by the CSTSK scheme of Fig. 1, yielding

$$\boldsymbol{S}(i)=s(i)\boldsymbol{A}(i), \tag{2}$$

TABLE I
EXAMPLE OF STSK MODULATION SCHEME, MAPPING 3 BITS PER SPACE-TIME BLOCK, WITH THE AID OF L–PSK CONSTELLATION

	$Q=1$ $\mathcal{L}=8$		$Q=2$ $\mathcal{L}=4$		$Q=4$ $\mathcal{L}=2$		$Q=8$ $\mathcal{L}=1$	
Input bits	$\boldsymbol{A}(i)$	$s(i)$	$\boldsymbol{A}(i)$	$s(i)$	$\boldsymbol{A}(i)$	$s(i)$	$\boldsymbol{A}(i)$	$s(i)$
000	$\boldsymbol{A}_1$	1	$\boldsymbol{A}_1$	1	$\boldsymbol{A}_1$	1	$\boldsymbol{A}_1$	1
001	$\boldsymbol{A}_1$	$e^{j\frac{\pi}{4}}$	$\boldsymbol{A}_1$	$e^{j\frac{\pi}{2}}$	$\boldsymbol{A}_1$	$e^{j\pi}$	$\boldsymbol{A}_2$	1
010	$\boldsymbol{A}_1$	$e^{j\frac{2\pi}{4}}$	$\boldsymbol{A}_1$	$e^{j\frac{2\pi}{2}}$	$\boldsymbol{A}_2$	1	$\boldsymbol{A}_3$	1
011	$\boldsymbol{A}_1$	$e^{j\frac{3\pi}{4}}$	$\boldsymbol{A}_1$	$e^{j\frac{3\pi}{2}}$	$\boldsymbol{A}_2$	$e^{j\pi}$	$\boldsymbol{A}_4$	1
100	$\boldsymbol{A}_1$	$e^{j\frac{4\pi}{4}}$	$\boldsymbol{A}_2$	1	$\boldsymbol{A}_3$	1	$\boldsymbol{A}_5$	1
101	$\boldsymbol{A}_1$	$e^{j\frac{5\pi}{4}}$	$\boldsymbol{A}_2$	$e^{j\frac{\pi}{2}}$	$\boldsymbol{A}_3$	$e^{j\pi}$	$\boldsymbol{A}_6$	1
110	$\boldsymbol{A}_1$	$e^{j\frac{6\pi}{4}}$	$\boldsymbol{A}_2$	$e^{j\frac{2\pi}{2}}$	$\boldsymbol{A}_4$	1	$\boldsymbol{A}_7$	1
111	$\boldsymbol{A}_1$	$e^{j\frac{7\pi}{4}}$	$\boldsymbol{A}_2$	$e^{j\frac{3\pi}{2}}$	$\boldsymbol{A}_4$	$e^{j\pi}$	$\boldsymbol{A}_8$	1

where $s(i)$ is the complex-valued symbol of the conventional modulation scheme employed, such as $\mathcal{L}$-PSK or $\mathcal{L}$-QAM, which is associated with $\log_2\mathcal{L}$ number of input bits. By contrast, the specific matrix $\boldsymbol{A}(i)$ is selected from the Q dispersion matrices $\boldsymbol{A}_q$ $(q=1,\cdots,Q)$ according to $\log_2 Q$ number of input bits. In this way, an additional means of transmitting further information bits was created. To be specific, we exemplify in Table I the mapping rule of our CSTSK modulation scheme, where a fixed number of $\log_2(Q\cdot\mathcal{L})=3$ bits per space-time block $\boldsymbol{S}(i)$ are transmitted by employing $\mathcal{L}$–PSK, for the specific cases of $(Q,\mathcal{L})=(1,8;2,4;4,2;8,1)$. As seen from Table I, there are several possible combinations of the number of dispersion matrices Q and of the constellation size $\mathcal{L}$, given 3 source bits per space-time block.

Moreover, the normalized throughput per time-slot (or per symbol) R of our STSK scheme may be expressed as

$$R=\frac{\log_2(Q\cdot\mathcal{L})}{T}\quad[\text{bits/symbol}]. \tag{3}$$

Having generated the space-time block $\boldsymbol{S}(i)$ to be transmitted, we then introduce the ML detection algorithm of our CSTSK scheme. By applying the vectorial stacking operation $vec()$ to the received signal block $\boldsymbol{Y}(i)$ in Eq. (1), we arrive at the linearized equivalent system model formulated as follows [14]:

$$\bar{\boldsymbol{Y}}(i)=\bar{\boldsymbol{H}}(i)\boldsymbol{\chi}\boldsymbol{K}(i)+\bar{\boldsymbol{V}}(i), \tag{4}$$

with the relations of

$$\bar{\boldsymbol{Y}}(i)=vec(\boldsymbol{Y}(i)) \quad \in\mathcal{C}^{NT\times 1}, \tag{5}$$
$$\bar{\boldsymbol{H}}(i)=\boldsymbol{I}\otimes\boldsymbol{H}(i) \quad \in\mathcal{C}^{NT\times MT}, \tag{6}$$
$$\bar{\boldsymbol{V}}(i)=vec(\boldsymbol{V}(i)) \quad \in\mathcal{C}^{NT\times 1}, \tag{7}$$
$$\boldsymbol{\chi}=[vec(\boldsymbol{A}_1)\cdots vec(\boldsymbol{A}_Q)] \in\mathcal{C}^{MT\times Q}, \tag{8}$$

where $\boldsymbol{I}$ is the identity matrix and $\otimes$ is the Kronecker product. Furthermore, the equivalent transmitted signal vector $\boldsymbol{K}(i)\in\mathcal{C}^{Q\times 1}$ is written as

$$\boldsymbol{K}(i)=[\underbrace{0,\cdots,0}_{q-1},s(i),\underbrace{0,\cdots,0}_{Q-q}]^{\mathrm{T}}, \tag{9}$$

where the modulated symbol $s(i)$ is situated in the qth element, noting that the index q corresponds to the index of the dispersion matrix $\boldsymbol{A}_q$ activated during the ith STSK block. Furthermore, the superscript $^{\mathrm{T}}$ is used to indicate the matrix transpose operation. Therefore, the number of legitimate transmit signal vectors $\boldsymbol{K}$ is given by $Q\cdot\mathcal{L}$. Additionally, in order to maintain a unity average transmission power for each STSK symbol duration, each of the Q dispersion matrices has to obey the power constraint of

$$\mathrm{tr}[\boldsymbol{A}_q^{\mathrm{H}}\boldsymbol{A}_q]=T\ (q=1,\cdots,Q), \tag{10}$$

where $\mathrm{tr}[\cdot]$ indicates the trace operation, while the superscript $^{\mathrm{H}}$ indicates the complex conjugate transpose operation. Our design rule used for generating the dispersion matrices $\boldsymbol{A}_q$ will be described in Section IV.

Since the equivalent system model of Eq. (4) is free from the effects of ICI, we can employ the single-antenna-based ML detector of [9], which imposes a low complexity. Let us consider that (q,l) correspond to the specific input bits of a STSK block, which are mapped to the lth $(l=1,\cdots,\mathcal{L})$ PSK symbol and qth $(q=1,\cdots,Q)$ dispersion matrix. Then the estimates $(\hat{q},\hat{l})$ are given by

$$(\hat{q},\hat{l}) = \arg\min_{q,l}||\bar{\boldsymbol{Y}}(i)-\bar{\boldsymbol{H}}(i)\boldsymbol{\chi}\boldsymbol{K}_{q,l}||^2 \tag{11}$$
$$= \arg\min_{q,l}||\bar{\boldsymbol{Y}}(i)-s_l\left(\bar{\boldsymbol{H}}(i)\boldsymbol{\chi}\right)_q||^2, \tag{12}$$

where s_l represents the lth symbol in the $\mathcal{L}$-point constellation and the signal vector $\boldsymbol{K}_{q,l}\in K$ $(1\le q\le Q,\ 1\le l\le\mathcal{L})$ indicates

$$\boldsymbol{K}_{q,l}=[\underbrace{0,\cdots,0}_{q-1},s_l,\underbrace{0,\cdots,0}_{Q-q}]^{\mathrm{T}}. \tag{13}$$

Furthermore, $\left(\bar{\boldsymbol{H}}(i)\boldsymbol{\chi}\right)_q$ is the qth column vector of the matrix $\bar{\boldsymbol{H}}(i)\boldsymbol{\chi}$. As mentioned in [9], this low-complexity ML detector exhibits the optimal detection performance in the uncoded scenario, where no *a priori* information is provided and the source bits are equi-probable. In the rest of this paper, we employ the parameter-based notation of our CSTSK scheme formulated as CSTSK(M,N,T,Q) for ease of treatment.

It should also be noted that while SM/SSK has to exponentially increase the number of transmit AEs for the sake of linearly increasing the number of transmitted input bits, our CSTSK scheme may circumvent this problem by increasing the number of dispersion matrices Q. Therefore, given an affordable tradeoff in terms of number of transmit antennas

M, our CSTSK scheme is capable of optimizing the derived transmission rate and diversity order in a more flexible and efficient manner by appropriately choosing T and Q.

B. Asynchronous CSTSK Scheme

As mentioned in [7]–[10], the SM and SSK schemes do not require any symbol-level time synchronization between the transmit antenna circuits, because a single antenna is activated at each symbol instant in these schemes. By contrast, our CSTSK scheme potentially requires IAS for the CSTSK's dispersion matrix activation, which replaces the antenna activation. However, by carefully designing the dispersion matrices $\boldsymbol{A}_q$ $(q = 1, \cdots, Q)$ of our CSTSK, we will present an Asynchronous CSTSK (A-CSTSK) arrangement dispensing with any IAS. More specifically, the structure of each dispersion matrix $\boldsymbol{A}_q$ is constructed so that there is a single non-zero element for each column of the dispersion matrix $\boldsymbol{A}_q$. This constraint enables us to avoid any simultaneous transmission by multiple antennas, similarly to the conventional SM and SSK schemes, while retaining all the benefits of our CSTSK scheme.

C. Differential STSK Scheme

The above-mentioned CSTSK scheme and the conventional SM/SSK scheme are both based on the *prior* knowledge of CSI and hence the performance degradation imposed by CSI estimation errors is unavoidable. To avoid this limitation, we proposed the corresponding DSTSK scheme as the extension of the CSTSK scheme with the aid of the Cayley unitary transform proposed in [6] and detailed in Section 8.4 of [1].

Fig. 2 shows the transmitter structure of our DSTSK scheme, where Q Hermitian matrices $\boldsymbol{A}_q$ $(q = 1, 2, \cdots, Q)$ are pre-allocated as the dispersion matrices prior to transmissions and $\mathcal{L}$-level Pulse Amplitude Modulation (PAM) is employed. Similarly to the CSTSK scheme of Fig. 1 and detailed in Section II-A, each space-time block contains $\log_2(Q \cdot \mathcal{L})$ source bits, where $\log_2 Q$ bits are mapped to $\boldsymbol{A}(i)$ using the previously outlined process of dispersion-matrix activation, while $\log_2 \mathcal{L}$ bits are mapped to the $\mathcal{L}$-PAM symbols $s(i)$. Thus, analogously to Eq. (2), the Hermitian matrix $\tilde{\boldsymbol{X}}(i) \in \mathcal{C}^{M \times T}$ is calculated as

$$\tilde{\boldsymbol{X}}(i) = s(i)\boldsymbol{A}(i), \tag{14}$$

where we have the relation of $M = T$. Furthermore, based on the Cayley unitary transform technique of [6], the Hermitian matrix $\tilde{\boldsymbol{X}}(i)$ is transformed to the unitary matrix $\boldsymbol{X}(i)$ as follows[3]

$$\boldsymbol{X}(i) = [\boldsymbol{I} - j\tilde{\boldsymbol{X}}(i)][\boldsymbol{I} + j\tilde{\boldsymbol{X}}(i)]^{-1}, \tag{15}$$

[3]We note that the Cayley unitary transform of Eq. (15) uniquely connects the unitary matrix $\boldsymbol{X}(i)$ with the Hermitian matrix $\tilde{\boldsymbol{X}}(i)$, therefore enabling the differential unitary encoding of Eq. (16) and leading to the linearized equivalent system model of Eq. (20). Furthermore, in order to ensure $\tilde{\boldsymbol{X}}(i)$ remains a Hermitian matrix, the modulated symbol $s(i)$ of Eq. (14) has to be a real-valued, rather than a complex-valued symbol, such as PSK and QAM. For this reason, we adopt a PAM constellation in our DSTSK scheme, although this may impose spectral inefficiency, due to the inapplicability of the complex-valued constellations.

where $\boldsymbol{I}$ is the identity matrix. Finally, the space-time matrix $\boldsymbol{S}(i)$ is differentially-encoded as follows:

$$\boldsymbol{S}(i) = \boldsymbol{S}(i-1) \cdot \boldsymbol{X}(i), \tag{16}$$

where the symbols in the mth row of $\boldsymbol{S}(i)$ are transmitted from the mth transmit AE over T symbol durations.

Assuming that the fading channel envelope remains constant over the two DSTSK block durations $2T$, the corresponding received signal block $\boldsymbol{Y}(i)$ of Eq. (1) is modified to

$$\begin{aligned}\boldsymbol{Y}(i) &= \boldsymbol{H}(i)\boldsymbol{S}(i) + \boldsymbol{V}(i) \\ &= \boldsymbol{Y}(i-1)\boldsymbol{X}(i) + \boldsymbol{V}(i) - \boldsymbol{V}(i-1)\boldsymbol{X}(i),\end{aligned} \tag{17}$$

which does not include any channel components. Instead of directly applying optimum ML detection to the received signal of Eq. (17), we introduce the linearization technique of [6] for the sake of facilitating the employment of the ML detector of Eq. (12). More specifically, upon multiplying both sides of Eq. (17) by $[\boldsymbol{I} + j\tilde{\boldsymbol{X}}(i)]$, we arrive at

$$\begin{aligned}\underbrace{\boldsymbol{Y}(i) - \boldsymbol{Y}(i-1)}_{\hat{\boldsymbol{Y}}(i)} &= \underbrace{-j[\boldsymbol{Y}(i) + \boldsymbol{Y}(i-1)]}_{\hat{\boldsymbol{H}}(i)}\tilde{\boldsymbol{X}}(i) \\ &+ \underbrace{\{-\boldsymbol{V}(i)[\boldsymbol{I} + j\tilde{\boldsymbol{X}}(i)] - \boldsymbol{V}(i-1)[\boldsymbol{I} - j\tilde{\boldsymbol{X}}(i)]\}}_{\hat{\boldsymbol{V}}(i)},\end{aligned} \tag{18}$$

where $\hat{\boldsymbol{Y}}(i)$ and $\hat{\boldsymbol{H}}(i)$ represent the equivalent received signals and the equivalent channel matrix, while the equivalent noise matrix $\hat{\boldsymbol{V}}(i)$ has independent columns with a covariance of

$$\hat{N}_0 = N_0(\boldsymbol{I} + \tilde{\boldsymbol{X}}^2). \tag{19}$$

Finally, by applying the $vec(\ )$ operation to Eq. (18), we arrive at [6]

$$\bar{\boldsymbol{Y}}(i) = \bar{\boldsymbol{H}}(i)\boldsymbol{\chi}\boldsymbol{K}(i) + \bar{\boldsymbol{V}}(i), \tag{20}$$

where we have

$$\bar{\boldsymbol{Y}}(i) = vec[\hat{\boldsymbol{Y}}(i)] \in \mathcal{C}^{NT \times 1} \tag{21}$$

$$\bar{\boldsymbol{H}}(i) = \boldsymbol{I} \otimes \hat{\boldsymbol{H}}(i) \in \mathcal{C}^{NT \times MT} \tag{22}$$

$$\bar{\boldsymbol{V}}(i) = vec[\hat{\boldsymbol{V}}(i)] \in \mathcal{C}^{NT \times 1}, \tag{23}$$

while $\boldsymbol{\chi}$ and $\boldsymbol{K}(i)$ are given by Eqs. (8) and (9), respectively, in the same manner as the CSTSK scheme of Section II-A.

Clearly, since the linearized system model of our DSTSK scheme (Eq. (20)) exhibits the same structure as for that of its CSTSK counterpart (Eq. (4)), we can readily invoke the single-antenna-based ML detector according to the criterion of Eq. (12), acknowledging that the resultant DSTSK's performance would inevitably suffer from the usual differential encoding induced SNR loss owing to the enhanced noise variance of Eq. (19).

As proposed in Section II-B for our CSTSK scheme, we can design the space-time block structure to dispense with IAS, which is achieved by appropriately restricting the search space of the dispersion matrix set $\boldsymbol{A}_q$ $(q = 1, \cdots, Q)$. Unfortunately, this technique cannot be applied to the DSTSK scheme and hence appropriate IAS is required.

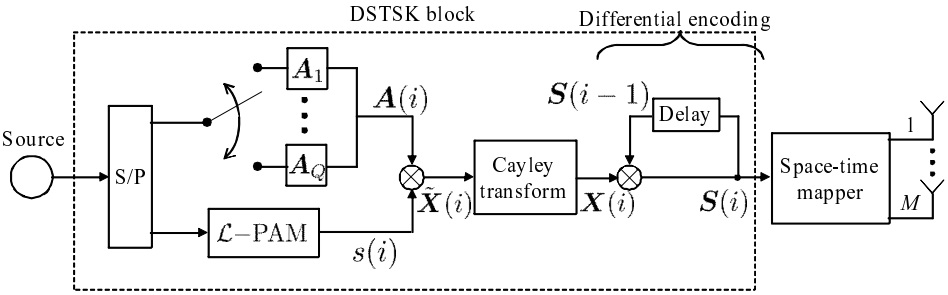

Fig. 2. Transmitter structure of our DSTSK scheme.

D. Computational Complexity

Let us now characterize the computational complexity imposed by the ML detection of our CSTSK scheme for both rapid and slow fading, which are given, respectively, by

$$\begin{cases} \dfrac{NTQ(4MT+6\mathcal{L})}{\log_2(Q\cdot\mathcal{L})}, & \text{(rapid fading)} \quad (24a) \\ \dfrac{NTQ[(4MT+4\mathcal{L})/\tau+2\mathcal{L}]}{\log_2(Q\cdot\mathcal{L})}. & \text{(slow fading)} \quad (24b) \end{cases}$$

Similarly, the complexity of our DSTSK scheme is represented by

$$\frac{NTQ(4MT+6\mathcal{L})}{\log_2(Q\cdot\mathcal{L})}. \tag{25}$$

Here, their complexity is evaluated in terms of the number of real-valued multiplications, noting that a single complex-valued multiplication was considered equivalent to four real-valued multiplications. For reference, the complexity of the SM/SSK scheme is also given by

$$\begin{cases} \dfrac{6MN\mathcal{L}}{\log_2(M\cdot\mathcal{L})}, & \text{(rapid fading)} \quad (26a) \\ \dfrac{(4/\tau+2)MN\mathcal{L}}{\log_2(M\cdot\mathcal{L})}. & \text{(slow fading)} \quad (26b) \end{cases}$$

Furthermore, τ represents an integer, quantifying the coherence block interval in slow fading environments. Although the SM/SSK scheme typically imposes a lower complexity than those of our CSTSK and DSTSK schemes, both the proposed schemes have a substantially lower complexity ML receiver in comparison to classic MIMO schemes, such as V-BLAST, LDCs and DLDCs, which is an explicit benefit of our ICI-free system model. Furthermore, the ratio of the STSK's complexity in Eq. (24a) over that of the SM/SSK scheme in Eq. (26a) is given by $TQ(4MT+6\mathcal{L})/6M\mathcal{L}$. Observe in this formula that an increase in the value of T gives rise to the quadratic increase of the above-mentioned complexity ratio. As a benefit, it may also potentially increase the attainable transmit diversity gain, as will be noted in Section II-E.

To be more specific, for the case of fast fading environments, the ML detector of our CSTSK scheme is required to calculate $\bar{\boldsymbol{H}}(i)\boldsymbol{\chi}\boldsymbol{K}_{q,l}$ $(1 \le q \le Q, 1 \le l \le \mathcal{L})$ for each CSTSK block, corresponding to the complexity of $NTQ(4MT+4\mathcal{L})/\log_2(Q\cdot\mathcal{L})$ out of $NTQ(4MT+6\mathcal{L})/\log_2(Q\cdot\mathcal{L})$ in Eq. (24a). On the other hand, in slow fading environments, this complexity is reduced to $NTQ(4MT+4\mathcal{L})/[\tau\log_2(Q\cdot\mathcal{L})]$, as shown in Eq. (24b), since the associated calculation can be reused within the channels' coherence time.

For our DSTSK scheme, the equivalent channels $\bar{\boldsymbol{H}}(i)\boldsymbol{\chi}$ have to be calculated for each DSTSK block, regardless of the value τ, as required by the implementation of differential decoding. However, it is worth mentioning that since our DSTSK scheme does not impose a pilot overhead and eliminates the complexity associated with CSI estimation, hence its complexity may be significantly lower than those of the CSTSK and SM/SSK schemes, especially when the corresponding MIMO channels change rapidly.

E. Maximum Achievable Diversity Order of CSTSK

For the general CSTSK block-based system model of Eq. (1), an upper bound of the average probability misinterpreting the transmitted space-time matrix $\boldsymbol{S}$ as $\boldsymbol{S}'$ is given by the Chernoff upper bound as follows: [15]

$$P(\boldsymbol{S}\to\boldsymbol{S}') \le \frac{1}{\left|\boldsymbol{I}_{M\cdot N}+\frac{1}{4N_0}\boldsymbol{R}\otimes\boldsymbol{I}_N\right|}, \tag{27}$$

where we have

$$\boldsymbol{R}=(\boldsymbol{S}-\boldsymbol{S}')(\boldsymbol{S}-\boldsymbol{S}')^{\mathrm{H}}. \tag{28}$$

Furthermore, for high SNRs, Eq. (27) may be simplified to [14]

$$P(\boldsymbol{S}\to\boldsymbol{S}') \le \frac{1}{[1/(4N_0)]^{m'N}\prod_{i=1}^{m'}\lambda_n^N}, \tag{29}$$

where m' and λ_n are the rank and the nth eigenvalue of $\boldsymbol{R}$, respectively. Let us now define the STC's diversity order as the exponent of its erroneous decision probability curve in Eq. (29). Then the resultant diversity order is determined by the smallest value of the product $m'N$ in Eq. (29). Therefore, we may conclude that the maximum achievable diversity order of our CSTSK scheme is given by $N\cdot\min(M,T)$, where $\min(M,T)$ corresponds to the achievable transmit diversity gain. This implies that upon increasing the CSTSK block duration T, the associated transmit diversity order increases, provided that the number of transmit antennas M satisfies $M \ge T$. In other words, increasing T beyond M does not result in any further transmit diversity improvement. By contrast, a lower T value may have the double-merits of a low computational complexity as well as of a high transmission rate, according to Eqs. (24a) and (3), although this is achieved at the cost of a reduced transmit diversity order.[4]

[4]The extreme example is the SM/SSK scheme, which may be considered as the CSTSK$(M,N,1,Q=M)$ scheme having the specific dispersion-matrix structure expressed as Eq. (36), where a high transmission rate as well as low complexity is achieved, at the expense of having no transmit diversity gain.

III. Three-stage Concatenated Turbo STSK Scheme

Let us invoke the turbo principle [12] to incorporate the proposed CSTSK and DSTSK schemes of Section II in a multiple-stage serially concatenated arrangement, for the sake of achieving a near-capacity performance. Furthermore, the iterative soft demapping principle is derived for our STSK scheme. Additionally, the capacity of our CSTSK scheme is also characterized.

A. System Overview

Fig. 3 shows the schematic of the proposed three-stage channel- and Unity Rate-Coded (URC) STSK scheme using iterative detection. Here, the input source bits are channel-encoded by a half-rate Recursive Systematic Convolutional (RSC) code and are interleaved by a random bit interleaver Π_1. Then, the interleaved bits are further encoded by a recursive URC encoder [16][5], and then the coded bits are interleaved by the second random interleaver Π_2 of Fig. 3. Finally, the interleaved bits are input to the CSTSK block of Fig. 1 or DSTSK block of Fig. 2, followed by the transmission of the space-time block $\boldsymbol{S}(i)$.

As illustrated in Fig. 3, a three-stage iterative decoding algorithm is employed at the receiver. To be specific, the Soft-Input Soft-Output (SISO) decoders of the receiver iteratively exchange soft extrinsic information in the form of Log Likelihood Ratios (LLRs). The CSTSK/DSTSK demapper block of Fig. 3 receives its input signals from the MIMO channels, which are combined with the extrinsic information provided by the URC decoder. Simultaneously, the URC decoder block of Fig. 3 receives extrinsic information both from the RSC channel decoder as well as from the CSTSK/DSTSK demapper and generates extrinsic information for both of its surrounding blocks seen in Fig. 3. The RSC channel decoder of Fig. 3 exchanges extrinsic information with the URC decoder and outputs the estimated bits after the I_{out} iterations. Here, the iterations between the CSTSK/DSTSK and URC decoder blocks are referred to as the inner iterations, while those between the URC and RSC decoders as outer iterations. The corresponding number of iterations are denoted by I_{in} and I_{out}, respectively. To be more specific, I_{in} inner iterations are implemented per each outer iteration, indicating that the total number of iterations becomes $I_{\text{in}} \cdot I_{\text{out}}$.

B. Soft CSTSK/DSTSK Demapper

Let us now detail the soft demapper of our CSTSK and DSTSK schemes. According to the equivalent system model of Eq. (4) derived for our CSTSK scheme, the conditional probability $p(\bar{\boldsymbol{Y}}|\boldsymbol{K}_{q,l})$ is given by

$$p(\bar{\boldsymbol{Y}}|\boldsymbol{K}_{q,l}) = \frac{1}{(\pi N_0)^{NT}} \exp\left(-\frac{||\bar{\boldsymbol{Y}} - \bar{\boldsymbol{H}}\boldsymbol{\chi}\boldsymbol{K}_{q,l}||^2}{N_0}\right). \quad (30)$$

Bearing in mind that the equivalent received signals $\bar{\boldsymbol{Y}}$ carry B channel-coded binary bits $\boldsymbol{b} = [b_1, b_2, \cdots, b_B]$, the resultant extrinsic LLR value of bit b_k for $k = 1, \cdots, B$ may be expressed as Eq. (31) [17] at the top of the next page, where K_1^k and K_0^k represent the sub-space of the legitimate equivalent signals K, satisfying $K_1^k \equiv \{\boldsymbol{K}_{q,l} \in K : b_k = 1\}$ and $K_0^k \equiv \{\boldsymbol{K}_{q,l} \in K : b_k = 0\}$, respectively, while $L_a(\cdot)$ represents the *a priori* information expressed in terms of the LLRs of the corresponding bits[6]. Furthermore, Eq. (31) is readily simplified by the max-log approximation [12], yielding:

$$L_{\text{e}}(b_k) = \max_{\boldsymbol{K}_{q,l} \in K_1^k} \left[-\frac{||\bar{\boldsymbol{Y}} - \bar{\boldsymbol{H}}\boldsymbol{\chi}\boldsymbol{K}_{q,l}||^2}{N_0} + \sum_{j \neq k} b_j L_a(b_j)\right] - \max_{\boldsymbol{K}_{q,l} \in K_0^k} \left[-\frac{||\bar{\boldsymbol{Y}} - \bar{\boldsymbol{H}}\boldsymbol{\chi}\boldsymbol{K}_{q,l}||^2}{N_0} + \sum_{j \neq k} b_j L_a(b_j)\right]. \quad (32)$$

Since the system models of Eq. (4) and of Eq. (20) exhibit a common structure, the soft CSTSK demapper of Eq. (31) or Eq. (32) may be also used for the soft DSTSK demapper by adjusting the noise variance component N_0.

C. Capacity of Our CSTSK Scheme

Here, we characterize the Discrete-input Continuous-output Memoryless Channel (DCMC) capacity [18] of the CSTSK scheme, which is defined for MIMO channels in combination with the specific multi-dimensional signaling set employed. Note that in contrast to the DCMC capacity, Shannon's channel capacity was defined for Continuous-input Continuous-output Memoryless Channels (CCMC) [19], assuming continuous-amplitude discrete-time Gaussian-distributed transmitted signals, where only the transmit power and the bandwidth are restricted.

According to [18], the DCMC capacity of our CSTSK scheme using $\mathcal{L}-$PSK or $\mathcal{L}-$QAM signaling may be expressed as

$$C = \frac{1}{T} \max_{p(\boldsymbol{K}_{1,1}), \cdots, p(\boldsymbol{K}_{Q,\mathcal{L}})} \sum_{q,l} \int_{-\infty}^{\infty} \cdots \int_{-\infty}^{\infty} p(\bar{\boldsymbol{Y}}|\boldsymbol{K}_{q,l}) p(\boldsymbol{K}_{q,l}) \cdot \log_2 \left[\frac{p(\bar{\boldsymbol{Y}}|\boldsymbol{K}_{q,l})}{\sum_{q',l'} p(\bar{\boldsymbol{Y}}|\boldsymbol{K}_{q',l'}) p(\boldsymbol{K}_{q',l'})}\right] d\bar{\boldsymbol{Y}} \quad \text{(bits/symbol)}. \quad (33)$$

Since Eq. (33) is maximized under the assumption that all the signals $\boldsymbol{K}_{q,l}$ are equi-probable, when we have $p(\boldsymbol{K}_{1,1}) = \cdots = p(\boldsymbol{K}_{Q,\mathcal{L}}) = 1/(Q \cdot \mathcal{L})$, Eq. (33) is simplified to [18]

$$C = \frac{1}{T}\left(\log_2(Q \cdot \mathcal{L}) - \frac{1}{Q \cdot \mathcal{L}} \times \sum_{q,l} \text{E}\left[\log_2\left\{\sum_{q',l'} \exp(\Psi_{q,l}^{q',l'})\middle| \boldsymbol{K}_{q',l'}\right\}\right]\right), \quad (34)$$

where we have

$$\Psi_{q,l}^{q',l'} = -||\bar{\boldsymbol{H}}\boldsymbol{\chi}(\boldsymbol{K}_{q,l} - \boldsymbol{K}_{q',l'}) + \bar{\boldsymbol{V}}||^2 + ||\bar{\boldsymbol{V}}||^2. \quad (35)$$

[5]The role of the URC is to impose an Infinite Impulse Response (IIR), which improves the achievable iterative decoding performance by efficiently spreading the extrinsic information, as detailed in [1].

[6]Here, the detailed calculations of the extrinsic LLRs output from the RSC and the URC decoders are omitted for the sake of space economy, noting that they can be found in [1] and the references therein.

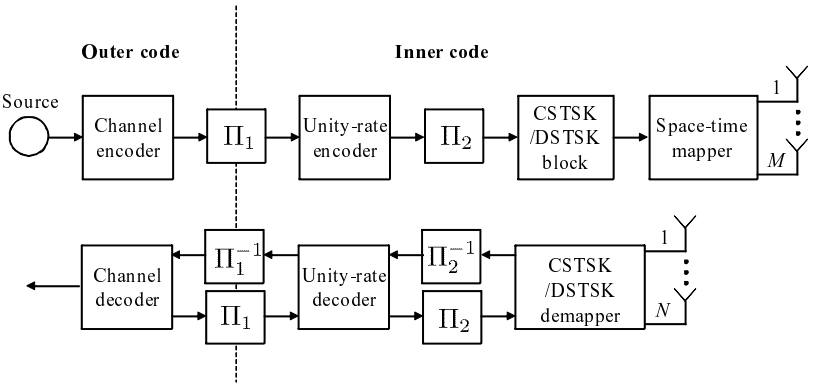

Fig. 3. Schematic of a three-stage RSC- and URC-coded coherent or differential STSK scheme using iterative detection.

$$L_{\rm e}(b_k) = \ln \frac{\sum_{\boldsymbol{K}_{q,l}\in K_1^k} p(\bar{\boldsymbol{Y}}|\boldsymbol{K}_{q,l}) \cdot \exp\left[\sum_{j\neq k} b_j L_a(b_j)\right]}{\sum_{\boldsymbol{K}_{q,l}\in K_0^k} p(\bar{\boldsymbol{Y}}|\boldsymbol{K}_{q,l}) \cdot \exp\left[\sum_{j\neq k} b_j L_a(b_j)\right]} = \ln \frac{\sum_{\boldsymbol{K}_{q,l}\in K_1^k} \exp\left[-||\bar{\boldsymbol{Y}} - \bar{\boldsymbol{H}}\boldsymbol{\chi}\boldsymbol{K}_{q,l}||^2/N_0 + \sum_{j\neq k} b_j L_a(b_j)\right]}{\sum_{\boldsymbol{K}_{q,l}\in K_0^k} \exp\left[-||\bar{\boldsymbol{Y}} - \bar{\boldsymbol{H}}\boldsymbol{\chi}\boldsymbol{K}_{q,l}||^2/N_0 + \sum_{j\neq k} b_j L_a(b_j)\right]}, \tag{31}$$

IV. Dispersion Matrix Properties and Design Criterion

A. Basic Properties

In our CSTSK and DSTSK schemes the specific design of the dispersion matrices $\boldsymbol{A}_q$ $(q = 1, \cdots, Q)$ significantly affects the achievable performance, similarly to those of LDC and DLDC schemes. More specifically, the dispersion matrices optimized for the LDC and DLDC schemes in [1] for example do not provide our CSTSK and DSTSK schemes with a high performance owing to their different system models. Here, let us note again that the dispersion matrices $\boldsymbol{A}_q$ $(q = 1, \cdots, Q)$ of our CSTSK(M, N, T, Q) scheme have the size of $(M \times T)$, each obeying the power constraints of Eq. (10), which are given by $\mathrm{tr}[\boldsymbol{A}_q^{\rm H}\boldsymbol{A}_q] = T$ $(q = 1, \cdots, Q)$. A meritorious dispersion-matrix set may exhibit a low correlation between any two of the space-time matrices $\boldsymbol{S} = s_l\boldsymbol{A}_q$ $(l \leq q \leq Q, 1 \leq l \leq \mathcal{L})$, which offers a good detection performance at the receiver.

To elaborate a little further, in Fig. 4 a group of DCMC capacity curves was recorded for our QPSK-modulated CSTSK$(2, N, 2, 4)$ and 8-PSK modulated CSTSK$(4, N, 2, 8)$ schemes designed for achieving transmission rates of $R = 2$ and $R = 3$ bits/symbol, respectively, where each dispersion matrix set $\boldsymbol{A}_q$ $(q = 1, \cdots, Q)$ was generated randomly. Here, we employed $N = 1$ or $N = 2$ receive antennas. We also characterized the SM schemes as benchmarkers, whose transmission rate R as well as number of receive and transmit antennas (M, N) correspond to those of each CSTSK arrangement. It can be seen in Fig. 4 that as expected, the achievable capacity substantially depends on the dispersion matrix set generated and hence optimization of the dispersion-matrix set is important.

Next, let us emphasize that our CSTSK scheme includes the SM/SSK arrangement as its special dispersion-matrix case. For

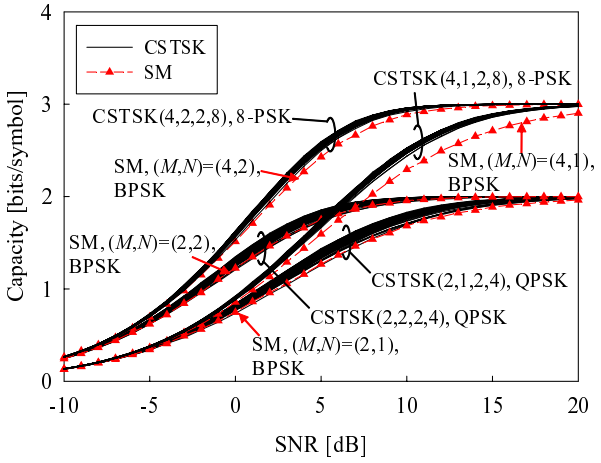

Fig. 4. A group of DCMC capacity curves of our QPSK-modulated CSTSK$(2, N, 2, 4)$ and 8-PSK modulated CSTSK$(4, N, 2, 8)$ schemes, achieving the transmission rates of $R = 2$ and $R = 3$ bits/symbol, respectively, while we employed $N = 1$ or $N = 2$ receive antennas. We also plotted the SM schemes as the benchmarkers, whose transmission rate R and number of receive and transmit antennas are corresponding to those of each CSTSK arrangement.

example, it is readily seen that CSTSK$(2, N, 1, 2)$ employing $\boldsymbol{A}_1 = [1\ 0]^{\rm T}$ and $\boldsymbol{A}_2 = [0\ 1]^{\rm T}$ is equivalent to the SM/SSK scheme assisted by $M = 2$ transmit antennas [8]. More generally, the CSTSK$(M, N, 1, Q = M)$ scheme having the dispersion matrices of

$$\boldsymbol{A}_1 = \begin{bmatrix} 1 \\ 0 \\ \vdots \\ 0 \end{bmatrix}, \boldsymbol{A}_2 = \begin{bmatrix} 0 \\ 1 \\ \vdots \\ 0 \end{bmatrix}, \cdots, \boldsymbol{A}_Q = \begin{bmatrix} 0 \\ 0 \\ \vdots \\ 1 \end{bmatrix} \tag{36}$$

exhibits a system structure, which is identical to that of the SM/SSK scheme employing (M, N) transmit and receive antennas, noting that in this case $\boldsymbol{\chi}$ becomes the identity matrix $\boldsymbol{I}$. Again, since in our CSTSK scheme the source bits are mapped to both the space and time-domain, rather than only to the spatial domain of the SM/SSK schemes [7]–[10], the SM/SSK arrangement is subsumed by our CSTSK scheme associated with $T = 1$, where mapping to the time dimension was deactivated. Furthermore, the generalized SSK scheme was presented in [20] as the extension of the SSK scheme, where multiple AEs are activated at each symbol interval, rather than a single one. This contributes to the enhancement of the transmission rate, which is achieved by simultaneous symbol transmissions from the different transmit AEs. This however imposes ICI, which may only be mitigated at the cost of an increased receiver complexity. We note that since the generalized SSK scheme does not exploit the time dimension similarly to the SM/SSK scheme, no transmit diversity gain can be achieved. In contrast to the generalized SSK scheme, our CSTSK arrangement remains unaffected by ICI and it is also capable of achieving a transmit diversity gain. Again, we note that in our CSTSK the equivalent receiver model of Eq. (4) does not exhibit any ICI, despite the fact that multiple antennas simultaneously transmit their signals. This is because only a single dispersion matrix $\boldsymbol{A}_q$ is activated in each block interval, which disperses a single symbol s_l across both the time- and space-dimensions.

B. Design Criterion

For our CSTSK scheme, the maximization of the DCMC capacity presented in Section III-C is adopted as the design criterion of the dispersion matrices $\boldsymbol{A}_q$, for the sake of maximizing the achievable capacity, given the constellation size $\mathcal{L}$ as well as the CSTSK parameters of (M, N, T, Q). An exhaustive search was implemented under the power constraint of Eq. (10). To be more specific, in the exhaustive search, Q dispersion matrices, each obeying the power constraint of Eq. (10), are randomly generated using the Gaussian distribution, and then the corresponding DCMC capacity is calculated based on Eq. (34). Once the random search process was repeated a certain number of times, the dispersion-matrix set exhibiting the highest DCMC capacity is chosen as the designed matrices. It is worth mentioning that the number of random search steps required to explore the entire legitimate search space depends both on the CSTSK parameters of (M, N, T, Q) as well as on the constellation size $\mathcal{L}$. As seen in Fig. 4, the DCMC capacity curves corresponding to different dispersion matrix sets typically did not exhibit a cross-over point and they converged to the same achievable transmission rate of R at high SNRs, implying that we can set a certain operational SNR point for the implementation of the exhaustive search.

More specifically, a set of dispersion matrices that we designed for the QPSK-modulated CSTSK$(2, 2, 2, 4)$ scheme are given by

$$\boldsymbol{A}_1 = \begin{bmatrix} 0.0002 + j0.1810 & 0.8053 + j0.0538 \\ -1.0650 - j0.3093 & -0.2929 + j0.0047 \end{bmatrix},$$

$$\boldsymbol{A}_2 = \begin{bmatrix} -0.0945 + j0.9968 & -0.6147 + j0.0826 \\ 0.1045 - j0.1268 & -0.7007 - j0.3077 \end{bmatrix},$$

$$\boldsymbol{A}_3 = \begin{bmatrix} -0.8263 - j0.2239 & 0.2992 + j0.6753 \\ 0.0804 + j0.0062 & -0.8362 + j0.1261 \end{bmatrix},$$

$$\boldsymbol{A}_4 = \begin{bmatrix} -0.4286 - j0.1219 & -0.4714 - j0.2877 \\ -0.5521 - j0.5868 & -0.0195 + j0.9203 \end{bmatrix},$$

where 100 000 random dispersion-matrix sets were tentatively generated. We note that these dispersion matrices will also be utilized for our numerical analysis conducted in Section V.

It was noted in the context of DLDCs [1] that the optimization of the DSTSK's dispersion matrix set $\boldsymbol{A}_q$ for maximizing the capacity is challenging and may lead to non-unique solutions. Therefore, we employ the well-known rank and determinant criterion of [21] for designing the dispersion matrix set $\boldsymbol{A}_q$ of our DSTSK scheme.

V. Performance Results

In this section we provide our performance results for characterizing both the uncoded and three-stage concatenated STSK schemes. Here, we assumed transmissions over Rayleigh block fading channels having a coherence time of T for our CSTSK scheme, which had a constant envelope over a CSTSK symbol, but faded independently between consecutive CSTSK blocks. By contrast, twice the coherence time of $2T$ was assumed for our DSTSK scheme.

A. Uncoded Scenario

Fig. 5 characterizes the achievable BER performance of our CSTSK system, comparing the effects of the number of dispersion matrices Q, where we also plotted the corresponding loose upper bound calculated from the simplified pairwise error probability of Eq. (29). Observe in Fig. 5 that upon increasing the value Q in our BPSK-modulated CSTSK$(2, 2, 2, Q)$ scheme from $Q = 1$ to $Q = 4$, the corresponding throughput increased from $R = 0.5$ bits/symbol to $R = 2.0$ bits/symbol, at the expense of a degraded BER performance, while maintaining a diversity order of four. Here, the upper bounds exhibited the exact achievable diversity order of four, although their BER values did not exactly match the simulated results.

Fig. 6 compares the achievable BER performance of our CSTSK$(M, 2, 2, 4)$ scheme and that of the corresponding SM scheme, where the employment of the optimum ML detector of [9] was assumed for the SM scheme. Here, we simulated two scenarios, where the first one considered the normalized throughput of $R = 2.0$ bits/symbol and $(M, N) = (2, 2)$ AEs, while the second one assumed $R = 3.0$ bits/symbol and $(M, N) = (4, 2)$. It was found that our CSTSK scheme outperformed the SM scheme in both the scenarios, although the advantage of our CSTSK scheme over the SM scheme was reduced upon increasing the number of dispersion matrices Q. More specifically, our CSTSK scheme achieved a diversity order of four, as a benefit of exploiting both the achievable transmit and receive diversity gains, while the SM scheme attained only a receive diversity order of two.

Furthermore, in Fig. 7 we compared the diverse CSTSK schemes with orthogonal STBCs, having the corresponding

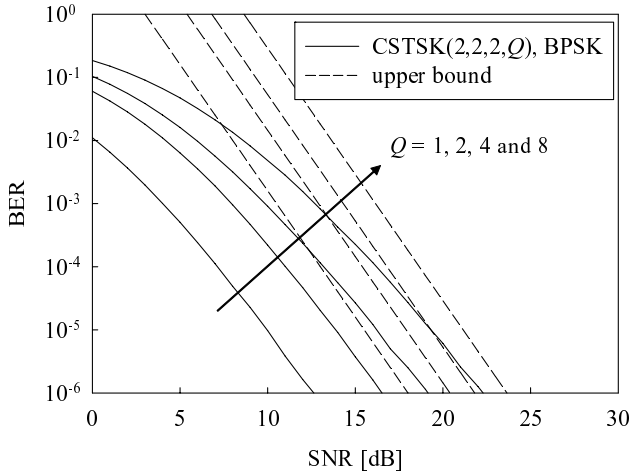

Fig. 5. Achievable BER curves of our CSTSK$(2, 2, 2, Q)$ system, comparing the effects of the number of dispersion matrices Q, where we also plotted the corresponding loose upper bound calculated from the simplified pairwise error probability of Eq. (29).

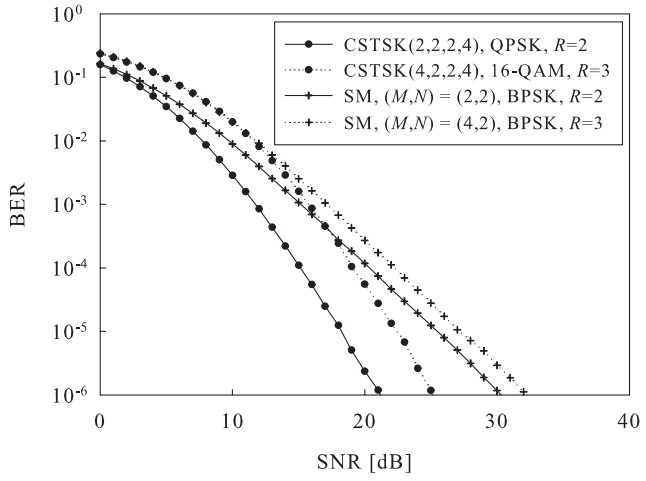

Fig. 6. Achievable BER curves of our CSTSK scheme and the SM scheme, for the cases of the employment of (M, N)=$(2, 2)$ antennas and of (M, N)=$(4, 2)$ antennas.

transmission rate R as well as the same number of transmit and receive antennas (M, N), such as $(M, N) = (3, 2)$ and $(M, N) = (4, 3)$. More specifically, we considered four different CSTSK arrangements, which are given by the QPSK-modulated CSTSK$(3, 2, 2, 4)$, the 8-PSK modulated CSTSK$(3, 2, 2, 8)$, the 8-PSK modulated CSTSK$(4, 3, 2, 8)$ and the 16-QAM CSTSK$(4, 3, 2, 16)$. Here, the classic G_3 and G_4 codes [22] were employed as benchmarkers. Observe in Fig. 7 that each of the CSTSK schemes outperformed the corresponding STBC benchmarker, due to the CSTSK's capability of striking a flexible rate-diversity tradeoff. We note that each CSTSK arrangement was designed for the relation of $M > T$, rather than for $M = T$, where we aimed for an enhanced transmission rate, at the cost of sacrificing the full diversity order.

Next, we investigated the achievable BER performance of our DSTSK scheme in Fig. 8, where we considered a 4–PAM assisted DSTSK$(2, 2, 2, 4)$ system, achieving a normalized

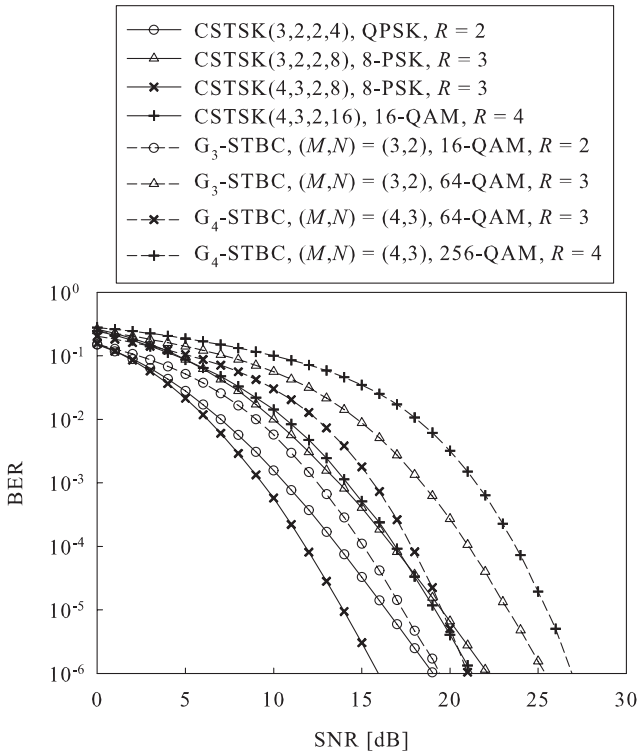

Fig. 7. Achievable BER curves of the diverse CSTSK schemes, compared with the orthogonal STBC schemes, having the identical transmission rate R as well as the number of transmit and the receive antennas (M, N), such as $(M, N) = (3, 2)$ and $(M, N) = (4, 3)$. Here, the classic G_3 and G_4 codes [22] were employed as the benchmarkers.

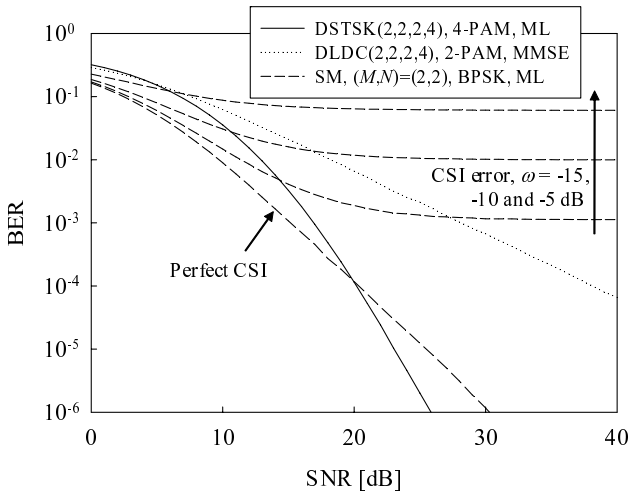

Fig. 8. Achievable BER curve of our DSTSK scheme, compared with the DLDC scheme as well as the SM scheme suffering from the CSI estimation error.

throughput of $R = 2.0$ bits/symbol. Here, we also plotted the BER curves of the SM schemes suffering from different levels of CSI estimation errors, where the estimated channels were contaminated by the additive Gaussian noise of $\mathcal{CN}(0, \omega)$ having a power of 5, 10 and 15 dB below the signal power, yielding equivalent SNRs of $\omega = -5$ dB, -10 dB and -15 dB. Furthermore, we employed the DLDC scheme of [6] as another benchmarker, where the MMSE criterion was

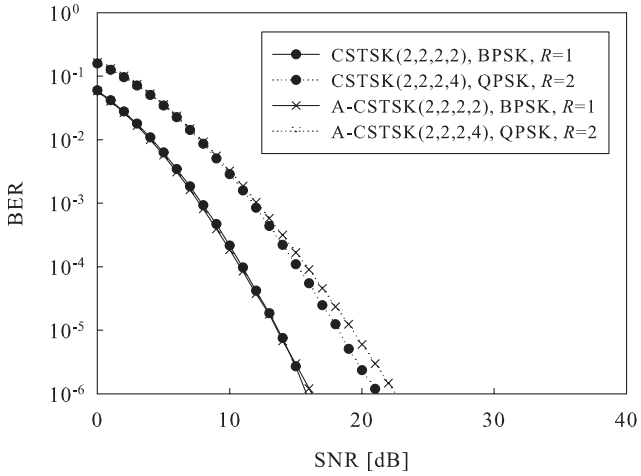

Fig. 9. Achievable BER curves of our CSTSK$(2, 2, 2, Q)$ scheme and of our A-CSTSK$(2, 2, 2, Q)$ scheme, while considering two scenarios, where one corresponds to $Q = 2$ dispersion matrices and BPSK modulation and the other employs $Q = 4$ dispersion matrices and QPSK modulation.

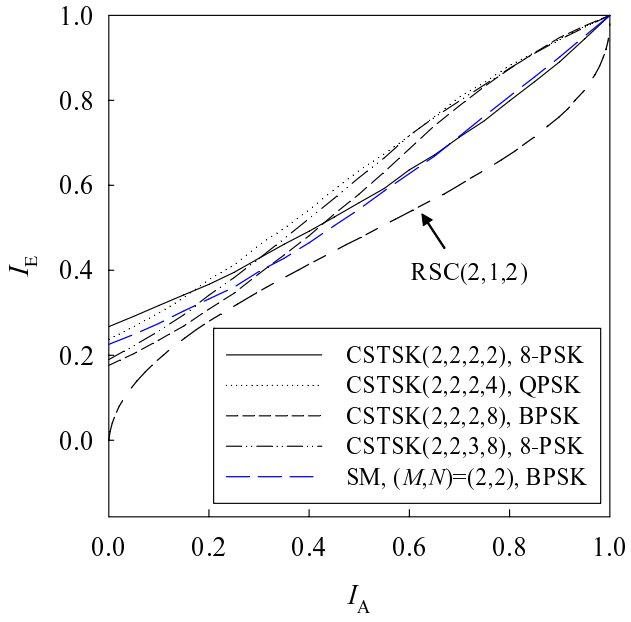

Fig. 10. EXIT chart of our CSTSK$(2, 2, T, Q)$ systems exhibiting the inner code rate of $R = 2.0$ bits/symbol, comparing different system parameters at SNR = -0.5 dB. The outer EXIT curve of the half-rate RSC$(2, 1, 2)$ code was also plotted.

employed for the DLDC's detection algorithm, noting that its complexity was higher than that of our DSTSK employing the single-antenna-based ML detector. Observe in Fig. 8 that as expected, our DSTSK scheme achieved a diversity order of four, hence outperforming both the DLDC scheme and the coherent SM scheme, which suffered from CSI estimation errors. Additionally, even for the case of no CSI error, the BER performance of our DSTSK scheme was better than that of the coherent SM scheme, when the SNR was higher than 20 dB.

Fig. 9 compares the achievable BER performance of our CSTSK scheme outlined in Section II-A and that of the A-CSTSK scheme of Section II-B, while considering both the BPSK-modulated STSK$(2, 2, 2, 2)$ and QPSK-modulated STSK$(2, 2, 2, 4)$ scenarios. Observe in Fig. 9 that upon increasing the number of dispersion matrices Q, the BER performance of the A-CSTSK scheme became slightly worse than that of the CSTSK scheme, owing to the restricted search space of the A-CSTSK's dispersion matrix set. However, our exhaustive simulation results not included here owing to space limitations demonstrated that the A-CSTSK scheme did not exhibit any significant performance degradation over the unconstrained CSTSK scheme.

B. Coded Scenario

Let us now continue by characterizing the performance of the iteratively detected STSK scheme, while investigating the effects of diverse parameters on the system with the aid of EXIT charts [17]. Again, the transmitter employed a half-rate RSC code having a constraint length of $\mathcal{K} = 2$ and octally represented generator polynomials of $(3, 2)_8$ as well as two random interleavers having lengths of $\Pi_1 = \Pi_2 = 200\,000$ bits. We also assumed that the number of inner and outer iterations was set to $I_{\rm in} = 2$ and $I_{\rm out} = 7$, respectively.

Fig. 10 shows the EXIT curves of four different PSK-modulated CSTSK$(2, 2, T, Q)$ systems having an uncoded throughput of 2.0 bits/symbol and an RSC-coded throughput of 1.0 bits/symbol, when considering SNR = -5 dB. Diverse system parameters, such as the constellation size $\mathcal{L}$, the number of dispersion matrices Q and the space-time block duration T were varied. Additionally, the EXIT curve of the identical-throughput SM scheme was also shown in Fig. 10. Furthermore, the EXIT curve of the RSC code employed in this paper was also plotted for reference. As seen in Fig. 10, all the inner-code EXIT curves reach the point of perfect convergence at $(I_{\rm A}, I_{\rm E})$ = (1.0, 1.0), as a benefit of the URC code's employment. It is clear that the EXIT curve shape of our CSTSK scheme varied, depending on the parameters chosen. The EXIT curve of the QPSK-modulated CSTSK$(2, 2, 2, 4)$ system exhibited the widest open tunnel among all the curves, including that of the SM scheme.

Furthermore, Fig. 11 shows the EXIT chart of our QPSK-modulated CSTSK$(2, 2, 2, 4)$ system, where the SNR was gradually increased from -2 dB to 3 dB in steps of 0.5 dB. Here, we also plotted the Monte-Carlo simulation based EXIT trajectory for the case of SNR = -0.5 dB. It was found in Fig. 11 that provided the SNR was higher than -1 dB, an open EXIT tunnel was exhibited and $I_{\rm out}$ = 7 outer iterations were necessary to converge to the $(I_{\rm A}, I_{\rm E})$ = (1.0, 1.0) point at SNR = -0.5 dB. Next, the corresponding CCMC and DCMC capacity curves of our CSTSK scheme and the DCMC capacity curve of the SM scheme are shown in Fig. 12. We also plotted the maximum achievable rates for our CSTSK scheme, which were calculated based on our EXIT chart results. More explicitly, it was shown in [23] and detailed in [1] that the maximum achievable rate $C_{\rm m}$ may be expressed as

$$C_{\rm m}({\rm SNR}) = R \cdot \mathcal{A}({\rm SNR}), \tag{37}$$

where $\mathcal{A}({\rm SNR})$ is the area under the inner decoder's EXIT curve corresponding to a certain SNR value. When employing

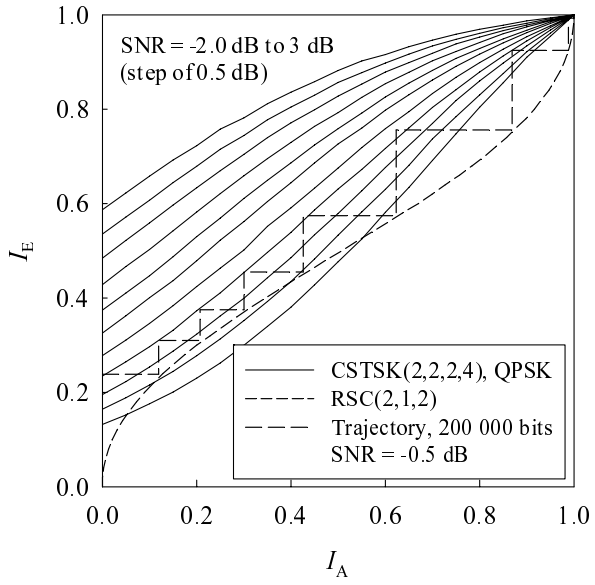

Fig. 11. EXIT chart of our QPSK-modulated CSTSK$(2, 2, 2, 4)$ system. The outer EXIT curve of the half-rate RSC$(2, 1, 2)$ code was also plotted.

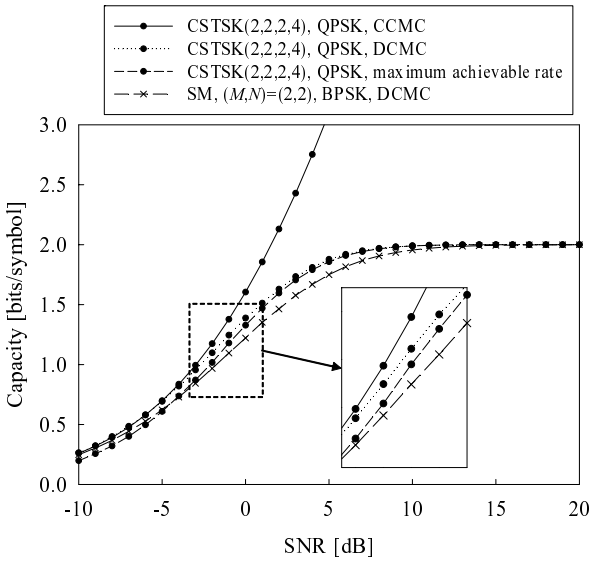

Fig. 12. Bandwidth efficiency of our CSTSK$(2, 2, 2, 4)$ system employing QPSK modulation, comparing the CCMC capacity, the DCMC capacity and the maximum achievable rate. The DCMC capacity of the BPSK-modulated SM employing $(M.N)$=$(2, 2)$ AEs was plotted as the benchmarker.

a half-rate RSC code, the CCMC and DCMC capacity limits of our QPSK-modulated CSTSK$(2, 2, 2, 4)$ system were found to be SNR = -3 dB and -2.7 dB, while the maximum achievable rate was attainable at SNR = -2.1 dB.

Finally, Fig. 13 illustrates the achievable BER performance of our RSC-coded and URC-coded CSTSK$(2, 2, 2, 4)$ arrangement with the aid of QPSK modulation. As predicted from the corresponding EXIT chart of Fig. 11, our CSTSK system exhibited an infinitesimally-low BER at SNR = -0.5 dB with the aid of $I_{\text{out}} = 7$ outer iterations, which was 1.6 dB away from the maximum achievable rate and 2.2 dB away from the DCMC capacity.

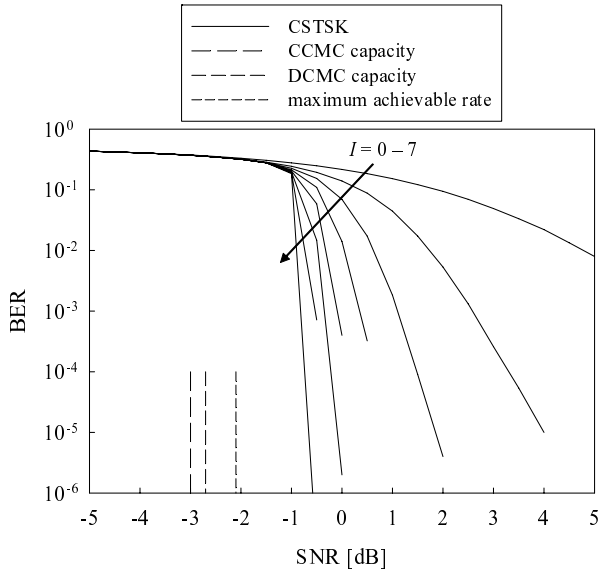

Fig. 13. Achievable BER performance of our RSC-coded and URC-coded CSTSK$(2, 2, 2, 4)$ with the aid of QPSK modulation, using interleaver lengths of $\Pi_1 = \Pi_2 = 200\,000$ bits.

VI. Conclusions

In this paper, inspired by the recently-proposed SM/SSK scheme, we conceived new coherent and differential STSK modulation schemes based on the novel concept of the dispersion matrix activation, which enables us to strike the required tradeoff between the MIMO's diversity and multiplexing gains. Since the resultant system model is not affected by ICI, we benefit from having low-complexity single-stream-based ML detection, similarly to the SM/SSK scheme. Furthermore, our DSTSK scheme, which is assisted by the Cayley unitary transform, does not require any CSI at the receiver, at the cost of the well-known 3-dB performance penalty in comparison to its coherent counterpart. The proposed STSK schemes may be viewed as the family of unified shift keying arrangements, including the recently-proposed SM and SSK schemes as their special cases. We also extended the CSTSK scheme to insure that no IAS is required between the RF branches associated with the transmit AEs, which led the so-called A-CSTSK scheme. Moreover, the proposed CSTSK and DSTSK schemes were incorporated in a three-stage serially concatenated arrangement for the sake of achieving a near-capacity performance, where the system parameters were optimized with the aid of EXIT charts. Our simulation results demonstrated that the STSK family has the potential of outperforming the conventional MIMO arrangements, such as the STBCs and the SM/SSK scheme, which is achieved by carefully designing the STSK's parameters, especially its dispersion matrices.

Lastly, for simplicity's sake we have adopted the exhaustive search method, in order to optimize the set of dispersion matrices. However, there are several approaches which may potentially simplify the exhaustive search, while achieving a comparable performance, similarly to the dispersion-matrix optimization of LDCs, although the detailed investigations are left for our future study.

REFERENCES

[1] L. Hanzo, O. Alamri, M. El-Hajjar, and N. Wu, *Near-Capacity Multi-Functional MIMO Systems: Sphere-Packing, Iterative Detection and Cooperation*. John Wiley and IEEE Press, 2009.

[2] P. Wolniansky, G. Foschini, G. Golden, and R. Valenzuela, "V-BLAST: an architecture for realizing very high data rates over the rich-scattering wireless channel," in *Proc. International Symp. Signals, Syst., Electron.*, Pisa, Italy, 1998, pp. 295-300.

[3] S. Alamouti, "A simple transmit diversity technique for wireless communications," *IEEE J. Sel. Areas Commun.*, vol. 16, no. 8, pp. 1451-1458, 1998.

[4] V. Tarokh, N. Seshadri, and A. Calderbank, "Space-time codes for high data rate wireless communication: performance criterion and code construction," *IEEE Trans. Inf. Theory*, vol. 44, no. 2, pp. 744-765, 1998.

[5] B. Hassibi and B. Hochwald, "High-rate codes that are linear in space and time," *IEEE Trans. Inf. Theory*, vol. 48, no. 7, pp. 1804-1824, 2002.

[6] ——, "Cayley differential unitary space-time codes," *IEEE Trans. Inf. Theory*, vol. 48, no. 6, pp. 1485-1503, 2002.

[7] R. Mesleh, H. Haas, C. Ahn, and S. Yun, "Spatial modulation—a new low complexity spectral efficiency enhancing technique," in *Proc. First International Conf. Commun. Netw.*, Beijing, China, Oct. 2006, pp. 1-5.

[8] R. Mesleh, H. Haas, S. Sinanovic, C. Ahn, and S. Yun, "Spatial modulation," *IEEE Trans. Veh. Technol.*, vol. 57, no. 4, pp. 2228-2242, 2008.

[9] J. Jeganathan, A. Ghrayeb, and L. Szczecinski, "Spatial modulation: optimal detection and performance analysis," *IEEE Commun. Lett.*, vol. 12, no. 8, pp. 545-547, 2008.

[10] J. Jeganathan, A. Ghrayeb, L. Szczecinski, and A. Ceron, "Space shift keying modulation for MIMO channels," *IEEE Trans. Wireless Commun.*, vol. 8, no. 7, pp. 3692-3703, 2009.

[11] M. Di Renzo and H. Haas, "Performance comparison of different spatial modulation schemes in correlated fading channels," in *Proc. IEEE International Conf. Commun.*, Cape Town, South Africa, May 2010, pp. 1-6.

[12] L. Hanzo, T. Liew, and B. Yeap, *Turbo Coding, Turbo Equalisation, and Space-Time Coding for Transmission over Fading Channels*. John Wiley and IEEE Press, 2002.

[13] A. Ashikhmin, G. Kramer, and S. Ten Brink, "Extrinsic information transfer functions: model and erasure channel properties," *IEEE Trans. Inf. Theory*, vol. 50, no. 11, pp. 2657-2673, 2004.

[14] R. Heath Jr and A. Paulraj, "Linear dispersion codes for MIMO systems based on frame theory," *IEEE Trans. Signal Process.*, vol. 50, no. 10, pp. 2429-2441, 2002.

[15] V. Tarokh, N. Seshadri, and A. Calderbank, "Space-time codes for high data rate wireless communication: performance criterion and code construction," *IEEE Trans. Inf. Theory*, vol. 44, no. 2, pp. 744-765, 1998.

[16] D. Divsalar, S. Dolinar, and F. Pollara, "Serial concatenated trellis coded modulation with rate-1 inner code," in *Proc. IEEE Global Telecommun. Conf.*, vol. 2, San Francisco, CA, Nov. 2000, pp. 777-782.

[17] S. ten Brink, "Convergence behavior of iteratively decoded parallel concatenated codes," *IEEE Trans. Commun.*, vol. 49, no. 10, pp. 1727-1737, 2001.

[18] S. Ng and L. Hanzo, "On the MIMO channel capacity of multidimensional signal sets," *IEEE Trans. Veh. Technol.*, vol. 55, no. 2, pp. 528-536, 2006.

[19] J. Proakis, *Digital Communications*. McGraw-Hill, 2001.

[20] J. Jeganathan, A. Ghrayeb, and L. Szczecinski, "Generalized space shift keying modulation for MIMO channels," in *Proc. IEEE 19th International Symp. Personal, Indoor Mobile Radio Commun.*, Cannes, France, Sep. 2008, pp. 1-5.

[21] V. Tarokh, S. Alamouti, and P. Poon, "New detection schemes for transmit diversity with no channel estimation," in *Proc. International Conf. Universal Personal Commun.*, vol. 2, 1998, pp. 917-920.

[22] V. Tarokh, H. Jafarkhani, and A. Calderbank, "Space-time block coding for wireless communications: performance results," *IEEE J. Sel. Areas Commun.*, vol. 17, no. 3, pp. 451-460, 1999.

[23] M. Tüchler, "Design of serially concatenated systems depending on the block length," *IEEE Trans. Commun.*, vol. 52, no. 2, pp. 209-218, 2004.

Shinya Sugiura (M'06) received the B.S. and M.S. degrees in aeronautics and astronautics from Kyoto University, Kyoto, Japan, in 2002 and 2004, respectively. In 2004, he joined Toyota Central Research and Development Laboratories (CRDL), Inc., Aichi, Japan. Since 2007 he has been with the School of Electronics and Computer Science, University of Southampton, Southampton, UK, on leave from Toyota CRDL Inc., where he is currently working towards the Ph.D. degree. His research has covered a range of areas in communications, including space-time modulation and demodulation, turbo coding, cooperative communications, multiuser detection, automotive antenna design as well as vehicular ad hoc networking. He has published over 20 research papers in various journals and conference proceedings. He was awarded IEEE AP-S Japan Chapter Young Engineer Award in December 2008.

Sheng Chen (M'90-SM'97-F'08) obtained a BEng degree from the East China Petroleum Institute, Dongying, China, in 1982, and a PhD degree from the City University, London, in 1986, both in control engineering. In 2005, he was awarded DSc from the University of Southampton, Southampton, UK. Since 1999 he has been with the School of Electronics and Computer Science, the University of Southampton, UK. He previously held research and academic appointments at the Universities of Sheffield, Edinburgh and Portsmouth, all in UK. Professor Chen's recent research works include adaptive signal processing, wireless communications, modelling and identification of nonlinear systems, neural network and machine learning, finite-precision digital controller design, evolutionary computation methods, and optimization. He has published over 280 research papers. In the database of the world's most highly cited researchers in various disciplines, compiled by Institute for Scientific Information (ISI) of the USA, Prof. Chen is on the list of the highly cited researchers in the engineering category, see http://www.ISIHighlyCited.com.

Lajos Hanzo (http://www-mobile.ecs.soton.ac.uk) FREng, FIEEE, FIET, DSc received his degree in electronics in 1976 and his doctorate in 1983. During his 34-year career in telecommunications he has held various research and academic posts in Hungary, Germany and the UK. Since 1986 he has been with the School of Electronics and Computer Science, University of Southampton, UK, where he holds the chair in telecommunications. He has co-authored 20 John Wiley - IEEE Press books on mobile radio communications totalling in excess of 10 000 pages, published 880 research papers and book chapters at IEEE Xplore, acted as TPC Chair of IEEE conferences, presented keynote lectures and been awarded a number of distinctions. Currently he is directing an academic research team, working on a range of research projects in the field of wireless multimedia communications sponsored by industry, the Engineering and Physical Sciences Research Council (EPSRC) UK, the European IST Programme and the Mobile Virtual Centre of Excellence (VCE), UK. He is an enthusiastic supporter of industrial and academic liaison and he offers a range of industrial courses. He is also an IEEE Distinguished Lecturer as well as a Governor of both the IEEE ComSoc and the VTS. He is the Editor-in-Chief of the IEEE Press and a Chaired Prof. also at Tsinghua University, Beijing. For further information on research in progress and associated publications please refer to http://www-mobile.ecs.soton.ac.uk